Atmos. Chem. Phys. Discuss., 9, 23755–23790, 2009
www.atmos-chem-phys-discuss.net/9/23755/2009/

Atmospheric
Chemistry
and Physics
Discussions

Alkyl nitrate production and persistence in the Mexico City Plume

A. E. Perring[1,*,], T. H. Bertram[1,***], D. K. Farmer[1,**], P. J. Wooldridge[1], J. Dibb[2], N. J. Blake[3], D. R. Blake[3], H. B. Singh[4], H. Fuelberg[5], G. Diskin[6], G. Sachse[6], and R. C. Cohen[1,7]**

[1]Department of Chemistry, University of California Berkeley, Berkeley, CA, USA
[2]Climate Change Research Institute, University of New Hampshire, Durham, NH, USA
[3]Department of Chemistry, University of California Irvine, Irvine, CA, USA
[4]NASA Ames Research Center, Moffett Field, CA, USA
[5]Department of Meteorology, Florida State University, Tallahassee, FL, USA
[6]NASA Langley Research Center, Hampton, VA, USA
[7]Department of Earth and Planetary Sciences, University of California Berkeley, Berkeley, CA, USA

Title Page
Abstract | Introduction
Conclusions | References
Tables | Figures
◀| | |▶
◀ | ▶
Back | Close
Full Screen / Esc
Printer-friendly Version
Interactive Discussion

[*] now at: National Oceanic and Atmospheric Administration, Earth System Research Laboratory, Chemical Sciences Division, Boulder, CO, USA
[**] now at: University of Colorado, Cooperative Institute for Research in Environmental Sciences, Boulder, CO, USA
[***] now at: Department of Chemistry and Biochemistry, University of California, San Diego, La Jolla, CA, USA

Received: 8 October 2009 – Accepted: 27 October 2009 – Published: 11 November 2009

Correspondence to: A. Perring (anne.perring@noaa.gov)

Published by Copernicus Publications on behalf of the European Geosciences Union.

Abstract

Alkyl and multifunctional nitrates (ΣANs) have been observed to be a significant fraction of NO_y in a number of different chemical regimes. Their formation is an important free radical chain termination step ending production of ozone and possibly affecting formation of secondary organic aerosol. ΣANs also represent a potentially large, unmeasured contribution to OH reactivity and are a major pathway for the removal of nitrogen oxides from the atmosphere. Numerous studies have investigated the role of nitrate formation from biogenic compounds. Less attention has been paid to the role ΣANs may play in the complex mixtures of hydrocarbons typical of urban settings. Measurements of ΣANs, NO_2, total peroxy nitrates (ΣPNs), HNO_3 and a wide suite of hydrocarbons were obtained from the NASA DC-8 aircraft during spring of 2006 in and around Mexico City and the Gulf of Mexico. ΣANs were observed to be 10–20% of NO_y in the Mexico City plume and to increase in importance with increased photochemical age. We describe three conclusions: 1) Correlations of ΣANs with odd-oxygen (O_x) indicate a stronger role for ΣANs in the photochemistry of Mexico City than is expected based on currently accepted photochemical mechanisms, 2) ΣAN formation suppresses peak ozone production rates by as much as 30% in the near-field of Mexico City and 3) ΣANs play a comparable role to ΣPNs in the export of NO_y to the Gulf Region.

1 Introduction

The chemistry of alkyl and multifunctional nitrates (molecules of the form $RONO_2$) acts to suppress O_3 formation in the near field of urban plumes and then to extend the range of ozone formation in the far field by releasing NO_x in locations far from NO_x emissions. However, there are few detailed observational tests capable of assessing the quantitative importance of these effects and current models incorporate contradictory assumptions about elements of the chemistry that are not well constrained by lab or by field observations. Recent analyses of models and their differences (Wu et al., 2007; Ito et al., 2007; Notaro et al., 2005), field observations (Perring et al., 2009a; Horowitz et al., 2007; Farmer and Cohen, 2008; Giacopelli et al., 2005; Farmer et al., 2009) and laboratory measurements (Paulot et al., 2009) have focused attention on the extent to which $RONO_2$ molecules preserve the $-ONO_2$ functional group upon oxidation. An emerging theme from these papers is that the lifetime of total $RONO_2$ ($\Sigma RONO_{2i}$, denoted ΣANs hereafter), rather than the lifetime of any individual $RONO_2$ molecule, is the key to understanding the effects of $RONO_2$ formation on atmospheric chemistry.

ΣANs have been observed to be a significant fraction of NO_y in a number of different chemical regimes (Rosen et al., 2004; Day et al., 2003; Cleary et al., 2005; Perring et al., 2009a) and have been inferred to be an important photochemical product in Mexico City with potential concentrations of several ppb (Dunlea et al., 2007). Here we present observations of ΣANs, measured by thermal dissociation coupled to laser-induced fluorescence detection of NO_2 (Thornton et al., 2000; Day et al., 2002), in and downwind of Mexico City using the NASA DC-8 platform during the Megacity Initiative: Local and Global Research Observations (MILAGRO) phase of the INTEX-B campaign in the spring of 2006. The aircraft flights targeted plume evolution and crossed the Mexico City plume at its origin and at distances as far as 1000 km downwind. We use these observations to explore the role of ΣANs as they affect ozone and nitrogen oxides. We show that ΣAN chemistry has important consequences for urban ozone (O_3) control strategies, for regional photochemistry and for the evolution of O_3 in the Mexico City plume. We examine aspects of the chemistry that are specific to this plume and discuss features that appear to be more generally applicable to any urban plume. We investigate the progression of the NO_y distribution as the plume ages with special attention to the continued significance of ΣANs as a fraction of NO_y.

2 Measurements

Observations described here were made aboard the NASA DC-8 during the Intercontinental Transport Experiment- Phase B (INTEX-B), which took place in the spring of 2006. INTEX-B, a NASA-led multi-partner atmospheric chemistry campaign, has been described elsewhere (Singh et al., 2009). One of the stated goals was to investigate the extent and persistence of Mexican pollution outflow as part of the MILAGRO campaign.

NO_2, ΣPNs, and ΣANs were measured using the Berkeley thermal dissociation-laser induced fluorescence instrument (Day et al., 2002; Thornton et al., 2000). Briefly, gas is pulled simultaneously through four channels consisting of heated quartz tubes maintained at specific temperatures for the dissociation of each class of compounds above. Each heated section is followed by a length of PFA tubing leading to a detection cell where NO_2 is measured using laser-induced fluorescence. Due to differing X-NO_2 bond strengths, ΣPNs, ΣANs and HNO_3 all thermally dissociate to NO_2 and a companion radical at a characteristic temperature. The ambient channel measures NO_2 alone, the second channel (180°C) measures NO_2 produced from the dissociation of ΣPNs in addition to ambient NO_2 so the observed signal is $NO_2 + \Sigma PNs$, the third channel (380°C) measures $NO_2 + \Sigma PNs + \Sigma ANs$, and the last channel (580°C) measures $NO_2 + \Sigma PNs + \Sigma ANs + HNO_3$. Concentrations of each class of compound correspond to the difference in NO_2 signal between two channels set at adjacent temperatures. The difference in NO_2 signal between the 180°C and the 380°C channel, for example, is the ΣANs mixing ratio. The instrument deployed for INTEX-B had a heated inlet tip that split in two immediately. Half of the flow was immediately introduced to heated quartz tubes for detection of ΣANs and HNO_3 while the other half was introduced to an additional heated quartz tube for detection of ΣPNs and an ambient temperature channel for detection of NO_2.

Ambient NO_2 and NO_2 produced by thermal dissociation was observed by laser-induced fluorescence as described in detail by Thornton et al. (2000). Briefly, a tunable dye laser is pumped at 7 kHz by a Q-switched, frequency doubled Nd^{+3}YAG laser.

The incoming gas is cooled through the use of a supersonic expansion (Cleary et al., 2002) and the dye laser, utilizing Pyrromethene 597 in isopropanol, is tuned to an isolated rovibronic feature of jet-cooled NO_2 at 585 nm. The frequency is held for 20 s at the peak of this feature and then for 5 s at an offline position in the continuum absorption. The ratio of peak to background fluorescence of the chosen feature is 10 to 1 at 1 atm and the difference between the two signals is directly proportional to the NO_2 mixing ratio. The laser light is focused in series through two multi-pass (White) cells (discussed in more detail below) and the red-shifted fluorescence is detected using a red-sensitive photomultiplier tube (Hamamatsu). Fluorescence counts are collected at 5 Hz, scattered light at wavelengths less than 700 nm is rejected by band-pass filters and time-gated detection is used to eliminate noise resulting from scattered laser light in the cell. We observe a dependence of NO_2 fluorescence on the external pressure. We calibrate the NO_2 LIF vs. altitude by direct measurement of NO_2 from a standard addition during a test-flight. Calibrations were performed at least once every two hours during a level flight leg using a 4.7 ppm NO_2 reference gas with a stated certainty of +/– 5%. The reference gas was compared to a library of standards in lab both before and after the campaign. The individual standards are compared on a regular basis (about every 6 months) to ensure stability and highlight when a given tank has degraded. These standards have been observed to remain stable for up to 5 years and to be accurate at atmospherically relevant mixing ratios to within 1% (Bertram et al., 2005).

The instrument deployed for INTEX-B had two detection cells. The direction of flow into the cell was controlled using a three-way valve and a bypass pump was used to maintain flow in the non-sampled channel. Cell 1 sampled either the ambient (75% of the time) or the 380°C channel (25% of the time) while cell 2 sampled either the 180°C (50% of the time) or the 580°C channel (50% of the time). Thus for every 2 min duty cycle there were three 20 s average measurements of NO_2, two 20 s average measurements of ΣPNs, one 20 s average measurement of ΣANs, one 20 s average measurement of HNO_3 and one 20 s average measurement of the sum (ΣPNs+ΣANs+HNO_3). As the ΣANs measurement is a subtraction, the uncertainty depends both on ΣANs and on the sum ($NO_2 + \Sigma PNs$). For example, if there were 100 ppt each of NO_2 and ΣPNs, the precision of the ΣANs measurement would be ~15 ppt in 20 s. If there were 1 ppb each of NO_2 and ΣPNs the precision of the ΣANs would be 40 ppt.

The TD-LIF measurement of HNO_3 has been shown to be the sum of aerosol and gas-phase HNO_3 (Fountoukis et al., 2009) and we expect aerosol phase organic nitrates to behave similarly. While a direct intercomparison of the ΣANs measurement has not been published, we have sampled pure standards of ethyl nitrate, propyl nitrate and isoprene nitrates (synthesized by wet chemical methods in the laboratory) in air. In each case we observe signal only in the ΣANs channel of the TD-LIF indicating that the nitrates are not dissociating in the other temperature channels. Comparison of TD-LIF observations of an isoprene nitrate standard to observations made using a PTR-MS show both instruments to be consistent to within 10% (Perring et al., 2009b). Comparisons of NO_2 and ΣPNs have also been described and indicate similar or better accuracy for these species (Thornton et al., 2003; Wooldridge et al., 2009; Fuchs et al., 2009).

HNO_3 was measured by the University of New Hampshire with a mist chamber followed by ion chromatography (Dibb et al., 1994). Hydrocarbons were measured by UC Irvine using gas chromatography of whole air samples (Colman et al., 2001). Oxygenated volatile organic carbon species (methyl-ethyl-ketone, methanol, ethanol, acetone and acetaldehyde collectively referred to, when combined with CH_2O, as oxidized volatile organic carbon or OVOC) were measured by NASA Ames using gas chromatography (Singh et al., 1999). NO (Georgia Tech) and O_3 (NASA Langley) were measured through chemiluminesence. OH and HO_2 were measured by laser-induced fluorescence by Penn State (Faloona et al., 2004). CH_2O was measured by NCAR using tunable diode laser absorption spectroscopy (TDLAS) (Fried et al., 2003) and by the University of Rhode Island (URI) using an enzyme-derivatization fluoresence technique following collection in an aqueous medium and high performance liquid chromatographic analysis (Heikes, 1992). URI also employed the enzyme-derivatization fluoresence technique to measure hydrogen peroxide (H_2O_2). Photolysis frequencies are calculated from spectraradiometer measurements as described by Shetter and Muller (1999). Ten-day back trajectories from locations of the DC-8 were calculated using the National Weather Service's Global Forecast Model (GFS) analyses of basic parameters as described by Fuelberg et al. (2007). The GFS data were available at 6 h intervals on a 1 degree latitude/longitude grid at 64 vertical levels.

The present work uses data from a 1-min merge available at http://www-air.larc.nasa.gov/missions/intex-b/intexb.html. We use back trajectories provided with the merged chemical data to select points that passed within ~100 miles (1.5 degrees) of the T0 site in the center of Mexico City at pressures higher than 680 mbar. The elevation of Mexico City is 2240 m and typical surface pressure is ~770 mbar. 680 mbar corresponds to an elevation of about 1km above ground level. Considering the 6 local flights out of Houston, there are a total of 2591 trajectories and, of those, 422 satisfy our criteria of having passed through the boundary layer in the vicinity of the Mexico City Metropolitan Area (MCMA).

3 Results and analysis

The formation of $RONO_2$ molecules occurs as a result of reactions between organic peroxy radicals (RO_2) and NO (Reaction R1a). The alternative to alkyl nitrate formation is propagation of the radical chain of events, conversion of NO to NO_2, and subsequent ozone production (Reaction R1b).

$$RO_2 + NO \rightarrow RONO_2 \tag{R1a}$$

$$RO_2 + NO \rightarrow RO + NO_2 \tag{R1b}$$

The ratio $k_{1a}/(k_{1a}+k_{1b})$ is α, the nitrate branching ratio. In this analysis, we examine the concentration of ΣANs and the fraction of NO_y that is represented by ΣANs as a function of time since emission of NO_x and VOC at the point of origin in downtown Mexico City. We discuss the evolving relationship between ΣANs and O_x (O_x=NO_2+O_3)

and place observational constraints on α. In Sect. 3.1 we develop a measure of airmass age. In Sect. 3.2 we describe the temporal evolution of NO_y partitioning in the plume, in Sect. 3.3 we describe the temporal evolution of the correlation of ΣAN with O_3 in the plume.

3.1 Photochemical age

We use the ratio of 2-butyl nitrate ($CH_3CHONO_2CH_2CH_3$) to butane, an indicator of time since last anthropogenic influence, to sort the MCMA plume points by increasing photochemical age. This indicator of age has been discussed previously by Bertman et al. (1995). Photochemical age indicators depend on the assumption that parent and daughter molecules, in this case a particular straight-chain alkane and its daughter alkyl nitrate, arise exclusively from a single chemical reaction (or a chain with a well-defined rate limiting step) and that the loss processes of the daughter are slower than the parent and well known. In addition, this analysis assumes that the emissions are effectively from a single isolated point source (LaFranchi et al., 2009). Depending on the accuracy required, mixing of a background into the plume must also be taken into account (Day et al., 2003). Neglecting mixing into a constant background doesn't affect the time ordering of the age indicator but does make its absolute magnitude less accurate.

In this case we choose butane and n-butyl nitrate as the parent-daughter pair. Ages calculated using ratios of pentyl nitrate to pentane give similar results. Neglecting mixing, and assuming that every RO_2 formed reacts with NO, the change in the concentration of a nitrate over time is then:

$$\frac{d[\mathrm{RONO_2}]}{dt} = \alpha \mathrm{k}_A[\mathrm{RH}] - \mathrm{k}_B[\mathrm{RONO_2}] \qquad (1)$$

where α is the nitrate branching ratio, $k_A = k_{OH+RH}$ *[OH] and $k_B = k_{OH+RONO_2}$*[OH] + J_{RONO_2}. The parameters for butane and butyl nitrate are taken from Bertman et al. (1995): $k_{OH+Butane} = 2.54\times10^{-12}$ cm^3/molecule/s, $k_{OH+2\ Butylnitrate}$ =

9.2×10^{-13} cm^3/molecule/s, $\alpha = 0.077$ and $J_{2\ \mathrm{Butylnitrate}} = 1.1\times10^{-6}\ \mathrm{s}^{-1}$ For the present calculation we have assumed OH=3×10^6 molecules/cm^2, a reasonable diurnal average concentration for the core of the Mexico City urban plume.

The above equation integrates to:

$$\frac{[\mathrm{RONO_2}]}{[\mathrm{RH}]} = \frac{\alpha k_A}{(k_A - k_B)}\left(1 - e^{(k_A - k_B)t}\right) - \frac{[\mathrm{RONO_2}]_0}{[\mathrm{RH}]_0} e^{(k_A - k_B)t} \qquad (2)$$

If we assume $[\mathrm{RONO_2}]_0 = 0$ and solve for t we find:

$$t = \frac{\ln\left(1 - \frac{[\mathrm{RONO_2}]}{[\mathrm{RH}]}\frac{(k_B - k_A)}{\alpha k_A}\right)}{(k_A - k_B)} \qquad (3)$$

Bertman et al. (1995) showed that these assumptions were adequate for evolving airmasses observed at Scotia Pennsylvania and the Kinterbish Wildlife Area, Alabama when applied to nitrates derived from hydrocarbons larger than propane.

Figure 1 shows the distance from T0 (panel a), the observed ratio of 2-buylnitrate to butane (panel b), the age calculated from the butylnitrate to butane ratio (panel c) and the observed NO_x to HNO_3 ratio (panel d) from a segment of the DC8's flight of 16 March 2006. The NO_x to HNO_3 ratio, which has also been widely employed as an indicator of photochemical processing, is expected to decrease with increased age as long as oxidation of NO_2 is more rapid than deposition of HNO_3. Figure 2 shows the calculated age of all points that have back trajectories that trace back to Mexico City and Fig. 3 shows the relationship between the calculated age and the distance to the T0 site in downtown Mexico City. Although we use a single value for OH in these calculations, it should also be noted that the rate of photochemical aging slows as the plume becomes more dilute and the OH concentration decreases. The OH concentration drops by more than a factor of 2 between the center of Mexico City and the Gulf of Mexico and this drives the shape of the curve shown in Fig. 3.

Much of the spread in the relationship between photochemical age and distance to the T0 site can be explained by variation in wind velocity. For example, the wind velocity below 4 km altitude (where most of the plume sampling occurred) on 16 March was ~5.5 m/s (blue points) while that on 19 March was ~10 m/s (red points). The higher wind velocity on the 19th carried the airmass farther from the source at equivalent photochemical aging than the mean. Note that the choice of OH concentration of 3×10^6 molecules/cm^3 gives photochemical ages in the first two days of plume evolution that are similar to the transport times calculated from observed wind speeds; i.e. on the day with a windspeed of 5.5 m/s the calculated photochemical age of the points near 1000 km is ~45 h while the transport time would be ~50 h. Additional spread in the transport time-photochemical time relationship is also introduced as a result of using a photochemical clock that turns off at night.

3.2 NO_y speciation in the Mexico City Plume

Figure 4a shows concentrations of the components of NO_y as a function of photochemical age and Fig. 4b shows NO_y speciation as a function of photochemical age. Near Mexico City (time < 5 h) NO_x is ~3.5 ppb and the dominant component of NO_y. Within 200 km (by ~15 h) NO_x decreases to <25% of NO_y and at the longest time considered (40 h) NO_x is 15% of NO_y, comparable to ΣPNs and ΣANs. HNO_3 is a minor fraction of NO_y (10%) close to Mexico City and increases to ~60% at the longest times.

The concentration of ΣPNs peaks at ~8 h and ΣPNs as a fraction of NO_y peak at ~15 h (100 km) where they account for 30% of NO_y after which they decrease to about ~15% of NO_y at ~40 h. Qualitatively this is the expected pattern. Previous analyses have shown that net production of peroxy nitrates occurs in the near-field of source regions where concentrations of NO_2 and RO_2 are high and the formation rate exceeds the rate of thermal decomposition. As the plume becomes more dilute, the formation rate will decrease exponentially while the thermal decomposition rate is determined only by the temperature. For urban plumes that experience rapid lofting and wet removal of both HNO_3 and ΣANs, ΣPNs become the dominant NO_y reservoir in the colder, lofted airmass (Altshuller, 1993; Singh and Salas, 1989; Talbot et al., 2003). The Mexico City Plume, as selected based on the criteria described above, was encountered exclusively below 5 km. The plume was almost entirely (95%) at temperatures above 280 K corresponding to a PAN thermal lifetime of less than 10 h. ΣANs start at 10% of NO_y near Mexico City. At the longest time they are of comparable importance to ΣPNs (~15% of NO_y). This indicates that chemical reactions of ΣANs may be important in the redistribution of reactive nitrogen within the Gulf of Mexico.

We can account, at least partially for dilution by comparing enhancements over the background to CO, which is a conserved tracer on the timescale of this plume study. Figure 5a shows fractional enhancement over the background for NO_y, CO, NO_x, ΣPNs and ΣANs. The fractional enhancement over background for species X is defined as:

$$\text{Fractional enhancement of species } X = (X - X_{\text{background}})/(X_{\text{initial}} - X_{\text{background}})$$

Where X_{initial} is the observed concentration of species X at less than 5 h of photochemical aging and $X_{\text{background}}$ is the observed concentration of species X at the longest photochemical ages over the Gulf of Mexico. CO on these timescales is a relatively inert tracer with an OH rate constant of 2.39×10^{-12} cm^3/molec/s (Sander et al., 2006) corresponding to a loss rate of 6%/day at OH=3×10^6 molecs/cm^3. The decay in CO is therefore primarily a measure of dilution. Molecules that decay faster than CO are removed by chemistry or deposition while those that decay more slowly are produced in the plume. Background concentrations used were 132 ppb for CO, 1.22 ppb for NO_y and as shown in Fig. 4a for the different NO_y species. The near identical dilution rate of NO_y to CO indicates that it was not subject to large depositional losses, consistent with the fact that the plume was primarily encountered between 2 and 4 km and should have been connected to the planetary boundary layer weakly if at all. Figure 5b shows the fractional enhancement of the components of NO_y divided by the fractional enhancement of CO, which should effectively cancel out the effect of dilution and allow us to examine the effect of chemistry. NO_x is initially enhanced relative to CO because dissociation of ΣPNs is a source of NO_x. Toward the end of the plume NO_x is depressed relative to CO because it has been converted to HNO_3. HNO_3 is chemically produced in the plume and thus lies above the dilution line. ΣANs behave similarly to HNO_3 confirming that they, too, continue to be produced as the plume ages. The lines all converge at the longest photochemical age because that is what we have defined as "background" conditions.

3.3 The evolution of the relationship between ΣANs and O_x

Since O_x and ΣANs arise from alternative channels of R1 the slope of the correlation of O_x and ΣANs is a measure of the balance between chain propagation (O_x production) and termination (ΣANs production) as long as losses of both are slow relative to production. Lower slopes imply a more significant role for ΣANs formation. Figure 6 shows the observed correlation between O_x and ΣANs at photochemical ages less than 5 h in red and at greater than 35 h in blue. The slope observed in the fresh plume (17 O_x/ΣAN) and the more aged plume (90 O_x/ΣAN) are shown by the solid lines. The dotted lines represent the slopes observed at intermediate age ranges (5–15 h, 15–25 h and 25–35 h) and show a gradual increase over time. The y-intercepts for the fits obtained for different photochemical ages are all similar (52.5±2.5 ppb O_x). It is therefore reasonable to assume a constant background for mixing with ΣAN levels that are low (0–50 ppt) and O_x that is 50–55 ppb. If the whole plume is being diluted into the same background mixture, then dilution will impact the observed concentrations of O_x and ΣANs but not affect the slope of the correlation.

The change in slope with time indicates a variable role for ΣAN production over the lifetime of the plume. Slopes of O_x/ΣANs have been reported for a number of different locations using ground-based ΣAN measurements in Granite Bay CA, Houston, TX, the Big Hill field site in the Sierra Foothills and using airborne measurements made over the southeastern US aboard the NASA DC-8. Typically lower O_x vs. ΣANs slopes are observed in urban locations than in more rural ones. For comparison with the current dataset, Rosen et al. (2004) found a slope of 29 O_x/ΣANs in the morning in Houston which increased to 41 in the afternoon and the average afternoon slope observed at the T1 site in Mexico City during MILAGRO was 22. Levels of ΣANs in remote areas of the troposphere have been observed to be very low and observed O_x/ΣANs slopes in the remote Pacific are found to be 200–500. This is higher than the slope found for even the longest times considered in the present analysis and illustrates the fact that the Mexico City plume impacts much of the Gulf region.

The instantaneous production rates of O_x and ΣANs which are given by:

$$P(O_x)_{\mathrm{inst}} = \Sigma_i \gamma_i (1-\alpha_i) k_{\mathrm{OH+RHi}}[\mathrm{OH}][\mathrm{RH}_i] \tag{4}$$

$$P(\Sigma ANs)_{\mathrm{inst}} = \Sigma_i \alpha_i k_{\mathrm{OH+RH}_i}[\mathrm{OH}][\mathrm{RH}_i] \tag{5}$$

where α_i is the nitrate branching ratio for RH_i and γ_i is the number of O_3 produced from the oxidation of RH_i. γ is equal to 2 for most hydrocarbons since R_{1b} typically results in the net production of 2 O_3 molecules; one from photolysis of the NO_2 formed directly and a second when subsequent alkoxy radical decomposition forms HO_2 and that HO_2 oxidizes NO to NO_2 followed by photolysis of that NO_2. See Rosen et al. (2004) for a more complete discussion of these equations. The variable slopes observed in the plume are the result of the integrated instantaneous production rates. While there is no simple analytical expression for the integrated production, in what follows we use the instantaneous production rates to asses whether we can explain the changes in the slope from point to point throughout the plume.

Taking the ratio of the two instantaneous production rates above we can find the relationship between the observed slope and the average branching ratio of the VOC mixture given by:

$$\frac{P(O_3)}{P(\Sigma \mathrm{ANs})} \equiv \frac{\bar{\gamma}\left(1-\bar{\alpha}\right)}{\bar{\alpha}} \approx \frac{2-2\bar{\alpha}}{\bar{\alpha}} \tag{6}$$

where ($\bar{\alpha}$) is the average branching ratio. A slope of 60 O_x/ΣAN for example, implies ($\bar{\alpha}$)= 3.2% while a slope of 20 implies ($\bar{\alpha}$)= 9.1%

Table 1 summarizes the values of α and k_{OH} used in this analysis, the median concentrations of each VOC considered within 5 h of Mexico City and the associated instantaneous production rates for O_3 and ΣANs. the calculated instantaneous O_x/ΣANs slope for each point is the ratio of the total P(O_x) (column 5) to the total P(ΣANs) (column 6). The calculated slope from Table 1 (for data within 5 h of Mexico City) is then ~60 O_x/ΣAN. Parallel calculations are performed for each of the different ranges of plume age. All rate constants and branching ratios are taken from the Leeds Master Chemical Mechanism. In addition to the 30 hydrocarbon species measured on-board the DC8, we have estimated concentrations of another 12 which are marked in the table by bold italic font. The nine unmeasured alkenes were estimated based on correlations with 1-butene observed at the T1 site. The three long-chain alkanes were estimated based on correlations with n-heptane observed in Houston. The estimated compounds add ~5% to P(O_3) and 13% to P(ΣANs). Note also that we have not included ΣANs themselves as precursor molecules in the initial calculations, as has been done previously (Rosen et al., 2004 and Cleary et al., 2005). The specific molecular structure of the nitrates will determine both their OH reactivites and di-nitrate branching ratios and the extreme variation in possible values for both of these parameters in the evolving plume makes them hard to approximate with a single value.

4 Discussion

4.1 ΣANs sources in Mexico City

The large $\overline{\alpha}$ implied by the small slope of the O_x/ΣANs correlation observed in and around Mexico City indicate a significant role for ΣANs in the photochemistry of the region. As described in Farmer et al. (2009), ΣAN formation at such high $\overline{\alpha}$ has a strong influence on O_3 formation rates. Given this large influence it would be valuable to understand the ΣAN source molecules in detail. There are large differences between the observed (17) and calculated (60) ΣANs vs. O_x slope near Mexico City, which implies the existence of unexplained photochemistry. This could be due to a combination of 1) the presence of unmeasured compounds with large nitrate branching ratios, 2) underestimates of currently accepted branching ratios for measured compounds, 3) a large component of di-nitrate formation from ΣANs.

Before further evaluation of these options it is useful to develop an independent check on the inferred $\overline{\alpha}$. One such independent check is to compare the observed ratio of $\Sigma(C_1-C_5$ nitrates)/ΣANs to the ratio calculated from the instantaneous production rate given by Eq. (5). Namely:

$$\left(\frac{\Sigma(C_1-C_5\,\text{nitrates})}{\Sigma\text{ANs}}\right)_{\text{calc}} \equiv \frac{\left(\sum_{j=C1}^{C5}\alpha_j * k_{OH+RH_j} * RH_j\right)}{\left(\sum_{i}\alpha_i * k_{OH+RH_i} * RH_i\right)} \tag{7}$$

where α_j and k_{OH+RHj} are reported branching ratios and OH rate constants for only the hydrocarbon precursors to the C_1-C_5 nitrates measured by GC and α_i and k_{OH+RH_i} are reported or estimated branching ratios and OH rate constants for the entire suite of observed hydrocarbons given in Table 1. $\Sigma(C_1-C_5$ nitrates) are predicted to be 27% of ΣANs in Mexico City based on the relative production rates but they were only observed to be 10%. As with the discrepancy between calculated and observed ΣANs vs. O_x slopes, this indicates an underestimate of ΣAN production.

First we consider the possibility of unmeasured nitrate precursors. A large burden of long-chain ($>C_{10}$) alkanes has been proposed based on observations of SOA in large urban centers and analysis of diesel exhaust (Robinson et al., 2007). Since long-chain alkanes have high nitrate formation branching ratios (~35%), adding them to our inventory could bring the observed and calculated branching ratios into agreement. A concentration of 0.5 ppb of a compound that reacted gas-kinetically with OH and had a branching ratio of 35% would result in a calculated O_x/ΣANs slope near Mexico City of 25 O_x/ΣAN (compared to the observed value of 17) and a calculated $\Sigma(C_1-C_5$ nitrate)/ΣANs ratio of 8% (compared to the observed value of 10%).

Title Page
Abstract | Introduction
Conclusions | References
Tables | Figures
◄◄ | ►►
◄ | ►
Back | Close
Full Screen / Esc
Printer-friendly Version
Interactive Discussion

A second possible explanation is that current estimates of nitrate branching ratios for some compounds that were measured are too low. Most notably, Mexico City is observed to have a large burden of aromatic compounds and there currently exists no aromatic oxidation experiment in the presence of NO_x that has shown carbon closure. The nitrate branching ratios used here are those used in MCM which are estimated using an expression proposed by Carter and Atkinson (1989). The full implementation of the MCMv3.1 aromatic oxidation scheme is described by Bloss et al. (2005). In addition to uncertainty in the yield of nitrates from the initial oxidation of aromatic compounds, there is a high degree of uncertainty in the yields of ring-opening v. ring-retaining products (Hamilton et al., 2003; Jenkin et al., 2003; Wagner et al., 2003; Wyche et al., 2009). The products of ring-opening pathways could themselves have high nitrate yields and significant nitrate formation could thus result from oxidation of the first-generation products of aromatic oxidation. A doubling of the nitrate branching ratio for all aromatic compounds would decrease the calculated ΣANs vs. O_x slope to 39 and the calculated $\Sigma(C_1-C_5$ nitrates)/ΣANs ratio to 22% which is an improvement. While uncertainties in nitrate formation from aromatic compounds alone cannot bring the calculations and observations into complete agreement, nitrate formation from aromatics and their oxidation products is significant in Mexico City and further study is warranted.

The third possibility is that ΣANs themselves are the unaccounted-for nitrate precursors. As noted above, they were not included in the initial calculation due to uncertainties in rate constants and branching ratios but it is highly likely that there is appreciable di-nitrate formation in the chemical environment of Mexico City. The calculations performed for datasets in Granite Bay and Houston assumed an OH rate constant of 1.6×10^{-11} cm^3/molecs/s and a branching ratio of 5%. If we include ΣANs in the calculation here using these parameters, the calculated ΣANs vs. O_x slope and $\Sigma(C_1-C_5$ nitrates)/ΣANs ratio are minimally changed. However, many of the 1st generation nitrates in Mexico City should be large molecules that retain at least one double bond. They may therefore react relatively quickly with OH and should have reasonably high branching ratios. If we assume that they have an OH rate constant of 7×10^{-11} cm^3/molecs/s, comparable to estimates of OH rate constants for isoprene nitrates (Perring et al., 2009a; Giacopelli et al., 2005) and a branching ratio of 17%, then the calculated ΣANs vs. O_x slope is 25 and the calculated $\Sigma(C_1-C_5$ nitrates)/ΣANs ratio is 0.08 which is comparable agreement to that achieved by the addition of 0.5 ppb of unmeasured long-chain hydrocarbons.

We should also note that the nighttime reaction of NO_3 with alkenes is known to give rise to ΣANs production without associated O_3 production (Warneke et al., 2004). The nitrate formation rate from NO_3-initiated oxidation is typically much higher than for OH-initiated oxidation and this reaction could represent a significant source of ΣANs. Based on concentrations of NO, NO_2 and O_3 observed at the T1 site in the hours before sunset (medians of 1 ppb, 8.6 ppb and 63 ppb respectively) and a nighttime temperature of 10°C, we calculate a possible total combined NO_3 and N_2O_5 (an NO_3 reservoir species) production of 1.4 ppb over the course of a typical night. Therefore, even if all of the available NO_3 were to react with alkenes with a 70% nitrate yield, it would lead to a maximum production of 1 ppb of ΣANs which is ~20% of observed daytime concentrations and would perturb the O_x vs. ΣANs slope by a similar amount, far smaller than the observed difference. In addition, significant nighttime concentrations (100's of ppts) of NO were observed at the T1 site at night, presumably due to local NO emissions. NO emissions would inhibit the accumulation of appreciable concentrations of NO_3 by titration. It is therefore likely that typical nighttime concentrations of NO_3 and N_2O_5 are substantially lower than the possible 1.4 ppb calculated above and that ΣANs production from NO_3 oxidation of alkenes is insignificant compared to typical daytime production rates of 0.3–0.5 ppb/h. Downwind of Mexico City, the possible nighttime production of NO_3 and N_2O_5 from observed NO_2 and O_3 is only a few ppt.

In summary, measured yields of ΣANs in Mexico City are high, corresponding to an average implied branching ratio of 7–10%, and are much larger than calculated based on observed VOC. We identify three poorly known quantities for reducing the modeled-measured difference: a) the presence of unmeasured, long-chain compounds with high yields, b) underestimates of nitrate yields from organic molecules and c) higher rates of dinitrate formation than have previously been considered in other locations and show that all of them are consistent with the data. All three should be subject to further investigation.

4.2 Evolution of the O_x vs. ΣANs correlation

The calculated and observed O_x vs. ΣANs can generally only be directly compared in the near-field of a source region where production outweighs all other factors. As the plume ages the most reactive primary VOC are depleted, enhancing secondary OVOC and resulting in a mixture that produces ozone and ΣANs in different ratios than the initial mixture does. These effects have been described previously for observations in Houston and Granite Bay where an increase in the slope of O_x/ΣANs (a decrease in α) over the course of the day was interpreted as due to the increase in non-nitrate producing ozone precursors. The slope was higher in the afternoon because of increased concentrations of O_3 precursors such as CO and CH_2O that are generated from the oxidation of other hydrocarbons but do not form nitrates upon oxidation. Similar processes are likely driving the variation in the slope of O_x/ΣANs in the Mexico City plume as it evolves downwind. In what follows we use the observed evolution of the O_x/ΣANs correlation and the $\Sigma(C_1-C_5$ nitrates)/ΣANs ratio in conjunction with the calculated instantaneous production rates to asses the spatial extent to which the plume is impacted by the unknown chemistry identified in Sect. 4.1.

Figure 7a shows the observed O_x vs. ΣANs slope as compared to that expected based on stepwise integration of the calculated instantaneous ΣANs and O_x production rates. The first point shown is a direct comparison of the calculated instantaneous O_x/ΣANs with the observed O_x/ΣANs correlation in Mexico City. We then calculate successive slopes by combining the observed slope at the earlier time with the instantaneous production rate at the later time. This prevents an error in the initial condition from propagating through the entire calculation. The calculated slope in Mexico City and just downwind is considerably higher than the observed slope but the agreement improves substantially by >30 h of photochemical aging. Again, we can corroborate this result using the ratio of $\Sigma(C_1-C_5$ nitrates)/ΣANs (Fig. 7b). The observed and calculated $\Sigma(C_1-C_5$ nitrates)/ΣANs ratios converge within 15 h. Thus, the compounds responsible for the excess ΣANs observed in Mexico City likely have short oxidative lifetimes and are consumed early in the plume evolution. Any of the above hypotheses would be consistent with this behavior.

4.3 Impacts of ΣANs chemistry on predicted O_3 production

The slope of O_x/ΣANs was observed to be remarkably high in Mexico City as compared to other urban locations (see also Farmer et al., 2009). As discussed above, the formation of alkyl and multifunctional nitrates affects our ability to predict ozone production both because it represents a direct alternative to the generation of NO_2 and thus O_3 from the RO_2 + NO reaction and because of the less direct feedback on RO_2 and HO_2 concentrations. ΣANs formation has not been evaluated in detail in the current generation of chemical models, a fact we suggest should be remedied in the near future. Any regional or global model, aimed at predicting O_3 concentrations, that fails to take this chemistry into account will overpredict O_3 production as a result. We can estimate the magnitude of this effect using observed radical species and a series of simple equations. The instantaneous gross O_3 production is defined as:

$$P(O_3) = [NO] \times \left(k_{NO+HO_2} \times [HO_2] + k_{NO+RO_2} \times [RO_2]\right) \tag{8}$$

We have measurements of NO and HO_2 and we can calculate RO_2 by using the conservation of radicals and setting $P(HO_x) = L(HO_x)$. HO_x production arises from the photolysis of O_3 in the presence of water, CH_2O and H_2O_2 with minor contributions from a number of oxygenated VOC's (OVOCs). For the analysis described here we have included photolysis of acetaldehyde, acetone, propanal, methanoic acid and HNO_3 to give an overall HO_x production rate of:

$$P(HO_x) = 2J_{O_3}[O_3]\frac{[H_2O]}{[M]} + 2J_{CH_2O\rightarrow H+HCO}[CH_2O] + 2J_{H_2O_2}[H_2O_2] + 2J_{Acetaldehyde}[CH_3CHO] + 2J_{Acetone}[CH_3C(O)CH_3] + 2J_{Propanal}[C_2H_5CHO] + 2J_{CH_3COOH}[CH_3COOH] + J_{HNO_3}[HNO_3] \quad (9)$$

HO_x loss occurs through production of HNO_3, ΣANs and organic peroxides (HOOH, ROOH or ROOR). Production of HNO_3 or an $RONO_2$ consumes a single HO_x molecule while production of a peroxide consumes two HO_x molecules so $L(HO_x)$ can be written as:

$$L(HO_x) = 2(k_{HO_2+HO_2}[HO_2]^2 + k_{RO_2+RO_2}[RO_2]^2 + k_{HO_2+RO_2}[HO_2][RO_2]) + k_{OH+NO_2}[OH][NO_2] + \alpha k_{RO_2+NO}[RO_2][NO] \quad (10)$$

Where α is the nitrate branching ratio. Setting $P(HO_x)=L(HO_x)$ and inserting measured values of OH, HO_2, NO and NO_2, we can solve the quadratic equation to find the RO_2 concentration. In what follows we have calculated RO_2 for each of the times for which we extracted an effective branching ratio in Sect. 3.3 above. Taking a water concentration of 6000 ppm, we use $k_{OH+NO2} = 1.22\times10^{-11}$ cm^3/molecs/s, $k_{HO_2+HO_2} = 2.74\times10^{-12}$ cm^3/molecs/s, $k_{HO_2+RO_2} = 8\times10^{-12}$cm^3/molecs/s and $k_{RO_2+RO_2} = 6.8\times10^{-14}$ cm^3/molecs/s based on JPL evaluation number 15 (Sander et al., 2006) assuming generic RO_2 behaves as $C_2H_5O_2$. It should be noted that the calculated RO_2 concentration and therefore the calculated $P(O_3)$ is sensitive to the assumed value of $k_{RO_2+RO_2}$. We use the median observed values of OH, HO_2, NO and NO_2 and calculate RO_2 concentrations using both the inferred α's and $\alpha=0$. We then use these RO_2 concentrations to calculate $P(O_3)$.

The top panel of Fig. 8 shows the percent change in calculated $P(O_3)$ as a result of including the formation of ΣANs. Near Mexico City, where alkyl nitrate production is high, the effect of including this chemistry in a model is to reduce the calculated $P(O_3)$ by 30%. The bottom panel of Fig. 8 shows $P(O_3)$ using $\alpha=0$ (blue squares and line) and using the α's inferred from the $O_x/\Sigma ANs$ correlation (green squares and line). The effect persists somewhat downwind of the city but the integrated effect of neglecting alkyl nitrate formation leads to significant errors in the calculated O_3 production over the lifetime of the megacity plume.

5 Conclusions

ΣANs have been observed to be a significant (∼10%) fraction of NO_y in the immediate vicinity and well downwind of Mexico City. Hundreds of ppt of ΣANs were observed over the Gulf of Mexico. The ΣANs fraction of NO_y increases with increasing photochemical age and indicates continued production of ΣANs far from the source region. The source of ΣANs is larger in the Mexico City plume than in other urban locations. The effect of ΣANs on calculated $P(O_3)$ is ∼30%, a value that is unexpectedly large and that implies careful consideration should be given to the role of ΣAN formation in discussion of any O_3 control strategies. We find that these observations of high ΣAN concentrations require one of more of the following: the presence of unmeasured, long-chain hydrocarbons with high nitrate formation rates, underestimates in nitrate formation rates for some fraction of the measured compounds, and/or a larger role for the formation of di-nitrates than has been considered previously. The evolution of the plume downwind indicates that the unknown compounds responsible are relatively short-lived.

Acknowledgements. The work presented here was funded by NASA headquarters under the NASA Earth Systems Science Fellowship Program and by NASA grant numbers NNG05GH196 and NNX08AE56G. The authors would also like to sincerely thank Brian Heikes, Alan Fried and Melody Avery for the use of their formaldehyde and ozone data and for their helpful comments on this manuscript.

References

Altshuller, A. P.: Pans In The Atmosphere, J. Air Waste Manage. Assoc., 43, 1221–1230, 1993.

Bertman, S. B., Roberts, J. M., Parrish, D. D., Buhr, M. P., Goldan, P. D., Kuster, W. C., Fehsenfeld, F. C., Montzka, S. A., and Westberg, H.: Evolution Of Alkyl Nitrates With Air-Mass Age, J. Geophys. Res.-Atmos., 100, 22805–22813, 1995.

Bertram, T. H., Cohen, R. C., Thorn, W. J., and Chu, P. M.: Consistency of ozone and nitrogen oxides standards at tropospherically relevant mixing ratios, J. Air Waste Manage. Assoc., 55, 1473–1479, 2005.

Bloss, C., Wagner, V., Jenkin, M. E., Volkamer, R., Bloss, W. J., Lee, J. D., Heard, D. E., Wirtz, K., Martin-Reviejo, M., Rea, G., Wenger, J. C., and Pilling, M. J.: Development of a detailed chemical mechanism (MCMv3.1) for the atmospheric oxidation of aromatic hydrocarbons, Atmos. Chem. Phys., 5, 641–664, 2005, http://www.atmos-chem-phys.net/5/641/2005/.

Carter, W. P. L. and Atkinson, R.: Alkyl nitrate formation from the atmospheric photooxidation of alkanes – a revised estimation method, J. Atmos. Chem., 8, 165–173, 1989.

Cleary, P. A., Wooldridge, P. J., and Cohen, R. C.: Laser-induced fluorescence detection of atmospheric NO_2 with a commercial diode laser and a supersonic expansion, Appl. Optics, 41, 6950–6956, 2002.

Cleary, P. A., Wooldridge, P. J., Day, D. A., Millet, D. B., McKay, M., Goldstein, A. H., and Cohen, R. C.: Observations of Total Alkyl nitrates within the Sacramento Urban Plume, Atmos. Chem. Phys. Discuss., 5, 4801–4843, 2005, http://www.atmos-chem-phys-discuss.net/5/4801/2005/.

Colman, J. J., Swanson, A. L., Meinardi, S., Sive, B. C., Blake, D. R., and Rowland, F. S.: Description of the analysis of a wide range of volatile organic compounds in whole air samples collected during PEM-Tropics A and B, Anal. Chem., 73, 3723–3731, 2001.

Day, D. A., Wooldridge, P. J., Dillon, M. B., Thornton, J. A., and Cohen, R. C.: A thermal dissociation laser-induced fluorescence instrument for in situ detection of NO_2, peroxy nitrates, alkyl nitrates, and HNO_3, J. Geophys. Res.-Atmos., 107, 4046, doi:10.1029/2001JD000779 2002.

Day, D. A., Dillon, M. B., Wooldridge, P. J., Thornton, J. A., Rosen, R. S., Wood, E. C., and Cohen, R. C.: On alkyl nitrates, O_3, and the "missing NO_y", J. Geophys. Res.-Atmos., 108, ACH7-1-10, 2003.

Dibb, J. E., Talbot, R. W., and Bergin, M. H.: Soluble acidic species in air and snow at Summit, Greenland, Geophys. Res. Lett., 21, 1627–1630, 1994.

Dunlea, E. J., Herndon, S. C., Nelson, D. D., Volkamer, R. M., San Martini, F., Sheehy, P. M., Zahniser, M. S., Shorter, J. H., Wormhoudt, J. C., Lamb, B. K., Allwine, E. J., Gaffney, J. S., Marley, N. A., Grutter, M., Marquez, C., Blanco, S., Cardenas, B., Retama, A., Villegas, C. R. R., Kolb, C. E., Molina, L. T., and Molina, M. J.: Evaluation of nitrogen dioxide chemiluminescence monitors in a polluted urban environment, Atmos. Chem. Phys., 7, 2691–2704, 2007, http://www.atmos-chem-phys.net/7/2691/2007/.

Faloona, I. C., Tan, D., Lesher, R. L., Hazen, N. L., Frame, C. L., Simpas, J. B., Harder, H., Martinez, M., Di Carlo, P., Ren, X. R., and Brune, W. H.: A laser-induced fluorescence instrument for detecting tropospheric OH and HO2: Characteristics and calibration, J. Atmos. Chem., 47, 139–167, 2004.

Farmer, D. K., and Cohen, R. C.: Observations of HNO_3, $\sum$AN, $\sum$PN and NO_2 fluxes: Evidence for rapid HO_x chemistry within a pine forest canopy, Atmos. Chem. Phys., 8, 3899-3917, 2008, http://www.atmos-chem-phys.net/8/3899/2008/.

Farmer, D. K., Perring, A. E., Wooldridge, P. J., Blake, D., Baker, A., Huey, G., Sjostedt, S., Tanner, D., de Gouw, J., Warneke, C., Kuster, W. C., and Cohen, R. C.: Urban air pollution: VOC controls are not orthogonal to NO_x, submitted to PNAS, October 2009.

Fountoukis, C., Nenes, A., Sullivan, A., Weber, R., Van Reken, T., Fischer, M., Matias, E., Moya, M., Farmer, D., and Cohen, R. C.: Thermodynamic characterization of Mexico City aerosol during MILAGRO 2006, Atmos. Chem. Phys., 9, 2141–2156, 2009, http://www.atmos-chem-phys.net/9/2141/2009/.

Fried, A., Crawford, J., Olson, J., Walega, J., Potter, W., Wert, B., Jordan, C., Anderson, B., Shetter, R., Lefer, B., Blake, D., Blake, N., Meinardi, S., Heikes, B., O'Sullivan, D., Snow, J., Fuelberg, H., Kiley, C. M., Sandholm, S., Tan, D., Sachse, G., Singh, H., Faloona, I., Harward, C. N., and Carmichael, G. R.: Airborne tunable diode laser measurements of formaldehyde during TRACE-P: Distributions and box model comparisons, J. Geophys. Res.-Atmos., 108, GTE19-1-23, 2003.

Fuchs, H., Ball, S. M., Bohn, B., Brauers, T., Cohen, R. C., Dorn, H. P., Dube, W. P., Fry, J. L., Haseler, R., Heitmann, U., Jones, R. L., Kleffman, J., Mentel, T. F., Muesgen, P., Rohrer, F., Rollins, A. W., Ruth, A. A., Kiendler-Scharr, A., Schlosser, E., Shillings, A. J. L., Tillmann, R., Varma, R. M., Venables, D. S., G., V. T., Wahner, A., Wegener, R., Wooldridge, P. J., and Brown, S. S.: Intercomparison measurements of NO_2 concentrations in the atmospheric simulation chamber SAPHIR during the NO3Comp campaign, Atmos. Meas. Tech., submitted, 2009.

Fuelberg, H. E., Porter, M. J., Kiley, C. M., Halland, J. J., and Morse, D.: Meteorological conditions and anomalies during the Intercontinental Chemical Transport Experiment-North America, J. Geophys. Res.-Atmos., 112, D12S06 doi:10.1029/2006jd007734, 2007.

Giacopelli, P., Ford, K., Espada, C., and Shepson, P. B.: Comparison of the measured and simulated isoprene nitrate distributions above a forest canopy, J. Geophys. Res.-Atmos., 110, D01304, doi:10.1029/2004JD005123, 2005.

Hamilton, J. F., Lewis, A. C., Bloss, C., Wagner, V., Henderson, A. P., Golding, B. T., Wirtz, K., Martin-Reviejo, M., and Pilling, M. J.: Measurements of photo-oxidation products from the reaction of a series of alkyl-benzenes with hydroxyl radicals during EXACT using comprehensive gas chromatography, Atmos. Chem. Phys., 3, 1999–2014, 2003, http://www.atmos-chem-phys.net/3/1999/2003/.

Heikes, B. G.: Formaldehyde And Hydroperoxides At Mauna-Loa Observatory, J. Geophys. Res.-Atmos., 97, 18001–18013, 1992.

Horowitz, L. W., Fiore, A. M., Milly, G. P., Cohen, R. C., Perring, A., Wooldridge, P. J., Hess, P. G., Emmons, L. K., and Lamarque, J. F.: Observational constraints on the chemistry of isoprene nitrates over the eastern United States, J. Geophys. Res.-Atmos., 112, D12S08, doi:10.1029/2006JD007747 2007.

Ito, A., Sillman, S., and Penner, J. E.: Effects of additional nonmethane volatile organic compounds, organic nitrates, and direct emissions of oxygenated organic species on global tropospheric chemistry, J. Geophys. Res.-Atmos., 112, D06309, doi:10.1029/2005JD006556, 2007.

Jenkin, M. E., Saunders, S. M., Wagner, V., and Pilling, M. J.: Protocol for the development of the Master Chemical Mechanism, MCM v3 (Part B): tropospheric degradation of aromatic volatile organic compounds, Atmos. Chem. Phys., 3, 181–193, 2003, http://www.atmos-chem-phys.net/3/181/2003/.

LaFranchi, B. W., Wolfe, G. M., Thornton, J. A., Harrold, S. A., Browne, E. C., Min, K. E., Wooldridge, P. J., Gilman, J. B., Kuster, W. C., Goldan, P. D., de Gouw, J., McKay, M., Goldstein, A. H., Ren, X., Mao, J. Q., and Cohen, R. C.: Closing the peroxy acetyl (PA) radical budget: observations of acyl peroxy nitrates (PAN, PPN and MPAN) during BEARPEX 2007, Atmos. Chem. Phys., 9, 7623–7641, 2009, http://www.atmos-chem-phys.net/9/7623/2009/.

Notaro, M., Liu, Z. Y., Gallimore, R., Vavrus, S. J., Kutzbach, J. E., Prentice, I. C., and Jacob, R. L.: Simulated and observed preindustrial to modern vegetation and climate changes, J. Clim., 18, 3650–3671, 2005.

Paulot, F., Crounse, J. D., Kjaergaard, H. G., Kroll, J. H., Seinfeld, J. H., and Wennberg, P. O.: Isoprene photooxidation: new insights into the production of acids and organic nitrates, Atmos. Chem. Phys., 9, 1479–1501, 2009, http://www.atmos-chem-phys.net/9/1479/2009/.

Perring, A. E., Bertram, T. H., Wooldridge, P. J., Fried, A., Heikes, B. G., Dibb, J., Crounse, J. D., Wennberg, P. O., Blake, N. J., Blake, D. R., Singh, H. B., and Cohen, R. C.: Airborne observations of total RONO2: New constraints on the yield and lifetime of isoprene nitrates, Atmos. Chem. Phys., 9, 1451–1463, 2009a, http://www.atmos-chem-phys.net/9/1451/2009/.

Perring, A. E., Wisthaler, A., Graus, M., Wooldridge, P. J., Lockwood, A. L., Mielke, L. H., Shepson, P. B., Hansel, A., and Cohen, R. C.: A product study of the isoprene+NO3 reaction, Atmos. Chem. Phys., 9, 4945–4956, 2009b, http://www.atmos-chem-phys.net/9/4945/2009/.

Robinson, A. L., Donahue, N. M., Shrivastava, M. K., Weitkamp, E. A., Sage, A. M., Grieshop, A. P., Lane, T. E., Pierce, J. R., and Pandis, S. N.: Rethinking organic aerosols: Semivolatile emissions and photochemical aging, Science, 315, 1259–1262, 2007.

Rosen, R. S., Wood, E. C., Wooldridge, P. J., Thornton, J. A., Day, D. A., Kuster, W., Williams, E. J., Jobson, B. T., and Cohen, R. C.: Observations of total alkyl nitrates during Texas Air Quality Study 2000: Implications for O_3 and alkyl nitrate photochemistry, J. Geophys. Res.-Atmos., 109, D07303, doi:10.1029/2003JD004227, 2004.

Sander, S. P., Finlayson-Pitts, B. J., Friedl, R. R., Golden, D. M., Huie, R. E., Keller-Rudek, H., Kolb, C. E., Kurylo, M. J., Molina, M. J., Moortgat, G. K., Orkin, V. L., Ravishankara, A. R., and Wine, P. H.: Chemical Kinetic and Photochemical Data for Use in Atmospheric Studies, Evaluation Number 15, 2006.

Shetter, R. E. and Muller, M.: Photolysis frequency measurements using actinic flux spectroradiometry during the PEM-Tropics mission: Instrumentation description and some results, J. Geophys. Res.-Atmos., 104, 5647–5661, 1999.

Singh, H. B. and Salas, L. J.: Measurements Of Peroxyacetyl Nitrate (Pan) And Peroxypropionyl Nitrate (Ppn) At Selected Urban, Rural And Remote Sites, Atmos. Environ., 23, 231-238, 1989.

Singh, H. B., Thompson, A. M., and Schlager, H.: SONEX airborne mission and coordinated POLINAT-2 activity: overview and accomplishments, Geophys. Res. Lett., 26, 3053–3056, 1999.

Talbot, R., Dibb, J., Scheuer, E., Seid, G., Russo, R., Sandholm, S., Tan, D., Singh, H., Blake, D., Blake, N., Atlas, E., Sachse, G., Jordan, C., and Avery, M.: Reactive nitrogen in Asian continental outflow over the western Pacific: Results from the NASA Transport and Chemical Evolution over the Pacific (TRACE-P) airborne mission, J. Geophys. Res.-Atmos., 108, 8803, doi:10.1029/2002JD003129, 2003.

Thornton, J. A., Wooldridge, P. J., and Cohen, R. C.: Atmospheric NO_2: In situ laser-induced fluorescence detection at parts per trillion mixing ratios, Anal. Chem., 72, 528–539, 2000.

Thornton, J. A., Wooldridge, P. J., Cohen, R. C., Williams, E. J., Hereid, D., Fehsenfeld, F. C., Stutz, J., and Alicke, B.: Comparisons of in situ and long path measurements of NO2 in urban plumes, J. Geophys. Res.-Atmos., 108, 2003.

Wagner, V., Jenkin, M. E., Saunders, S. M., Stanton, J., Wirtz, K., and Pilling, M. J.: Modelling of the photooxidation of toluene: conceptual ideas for validating detailed mechanisms, Atmos. Chem. Phys., 3, 89–106, 2003, http://www.atmos-chem-phys.net/3/89/2003/.

Warneke, C., de Gouw, J. A., Goldan, P. D., Kuster, W. C., Williams, E. J., Lerner, B. M., Jakoubek, R., Brown, S. S., Stark, H., Aldener, M., Ravishankara, A. R., Roberts, J. M., Marchewka, M., Bertman, S., Sueper, D. T., McKeen, S. A., Meagher, J. F., and Fehsenfeld, F. C.: Comparison of daytime and nighttime oxidation of biogenic and anthropogenic VOCs along the New England coast in summer during New England Air Quality Study 2002, J. Geophys. Res.-Atmos., 109, D10309, doi:10.1029/2003JD004424, 2004.

Wooldridge, P. J., Perring, A. E., Bertram, T. H., Thornton, J. A., LaFranchi, B. W., Roberts, J. M., Huey, L. G., and Cohen, R. C.: Comparison of TD-LIF total peroxynitrate measurements to the sum of individual GC and COMS measurements of peroxyacyl nitrates, Atmos. Meas. Tech., in preparation, 2009.

Wu, S. L., Mickley, L. J., Jacob, D. J., Logan, J. A., Yantosca, R. M., and Rind, D.: Why are there large differences between models in global budgets of tropospheric ozone?, J. Geophys. Res.-Atmos., 112, D05302, doi:10.1029/2006JD007801, 2007.

Wyche, K. P., Monks, P. S., Ellis, A. M., Cordell, R. L., Parker, A. E., Whyte, C., Metzger, A., Dommen, J., Duplissy, J., Prevot, A. S. H., Baltensperger, U., Rickard, A. R., and Wulfert, F.: Gas phase precursors to anthropogenic secondary organic aerosol: detailed observations of 1,3,5-trimethylbenzene photooxidation, Atmos. Chem. Phys., 9, 635–665, 2009, http://www.atmos-chem-phys.net/9/635/2009/.

Table 1. Columns 2 and 3 show OH rate constants and nitrate branching ratios for the suite of hydrocarbons observed in Mexico City (listed in column 1). Columns 3–6 show the median concentrations and the associated ozone and alkyl nitrate production rates respectively. Italics indicate compounds for which concentrations were estimated rather than measured as described in the text.

	kOH (cm^3 $molecule^{-1}$ s^{-1})	alpha	Concentration (ppt)	P(O_3) (ppt/h)	P(ANs) (ppt/h)
Alkanes					
Methane	6.34E-15	0.001	1 969 000	701	0.35
Ethane	2.58E-13	0.009	2966	43	0.19
Propane	1.10E-12	0.036	20 697	1279	23.01
nButane	2.54E-12	0.083	8022	1144	47.49
nPentane	4.00E-12	0.123	1809	406	24.99
iButane	2.19E-12	0.027	2553	314	4.24
iPentane	3.90E-12	0.075	3625	794	29.77
2-Methylpentane	5.30E-12	0.111	1004	299	16.59
3-Methylpentane	5.40E-12	0.109	628	190	10.38
Hexane	5.45E-12	0.212	753	230	24.43
Heptane	7.02E-12	0.278	217	86	11.89
Octane	8.71E-12	0.346	*109*	*53*	*9.22*
Nonane	9.99E-12	0.393	*54*	*30*	*5.95*
Decane	1.12E-11	0.417	*54*	*34*	*7.08*
Alkenes					
Ethene	8.20E-12	0.0005	3999	1842	0.46
Propene	2.63E-11	0.021	432	638	6.70
1-Butene	3.14E-11	0.039	73	129	2.51
Butadiene	6.66E-11	0.065	5	19	0.61
Isoprene	1.01E-10	0.07	23	130	4.57
Methylpropene	5.14E-11	0.012	*45*	*130*	*0.78*
2-Methyl 1-butene	6.07E-11	0.02	*45*	*153*	*1.53*
3-Methyl 1-butene	3.18E-11	0.059	*11*	*20*	*0.58*
2-Mehtyl 2-butene	8.69E-11	0.034	*34*	*166*	*2.82*
trans 2-Butene	6.40E-11	0.041	*51*	*183*	*3.76*
cis 2-Butene	5.64E-11	0.041	*30*	*95*	*1.95*
1-Pentene	3.14E-11	0.059	*49*	*86*	*2.55*
trans 2-Pentene	6.70E-11	0.064	*42*	*158*	*5.06*
cic 2-Pentene	6.50E-11	0.064	*18*	*66*	*2.10*
Aromatics					
Benzene	1.22E-12	0.029	851	58	0.85
Ethylbenzene	7.00E-12	0.072	290	114	4.10
Propylbenzene	5.80E-12	0.093	39	13	0.59
Toluene	5.96E-12	0.079	3805	1274	50.31
3-Ethyltoluene	1.86E-11	0.094	86	90	4.22
4-Ethyltoluene	1.18E-11	0.137	34	23	1.54
O-Xylene	1.36E-11	0.081	197	150	6.09
M-Xylene	2.30E-11	0.074	250	323	11.95
P-Xylene	1.43E-11	0.097	141	113	5.49
1,3,5-Trimethylbenzene	5.76E-11	0.127	5	16	1.03
1,2,4-Trimethylbenzene	3.25E-11	0.105	93	170	8.91
Other					
CO	2.39E-13	0	600 000	4027	0.00
H_2CO	8.37E-12	0	7793	1832	0.00
Acetaldehyde	1.58E-11	0	2497	2216	0.00
Total				19 836	347

Title Page
Abstract
Introduction
Conclusions
References
Tables
Figures
◀|
|▶
◀
▶
Back
Close
Full Screen / Esc
Printer-friendly Version
Interactive Discussion

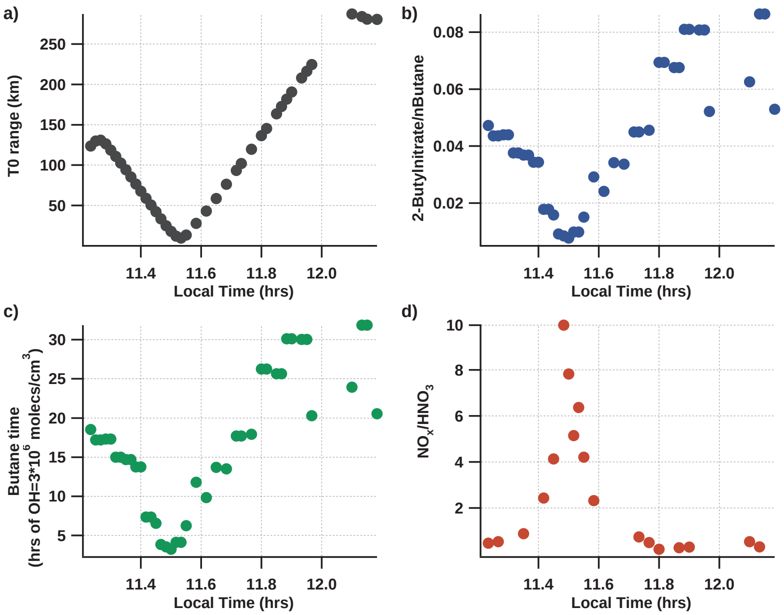

Fig. 1. An example from the DC8 Flight #7 of 16 March 2006 of the variation of several indicators of chemical age with distance from the center of Mexico City. Panel **(a)** shows the distance to Mexico City as a function of time, panel **(b)** shows the ratio of 2-Butyl nitrate to n-Butane, panel **(c)** shows the calculated photochemical age in hours at OH=3×10^6 molecs/cm^3 and panel **(d)** shows the ratio of NO_x to HNO_3.

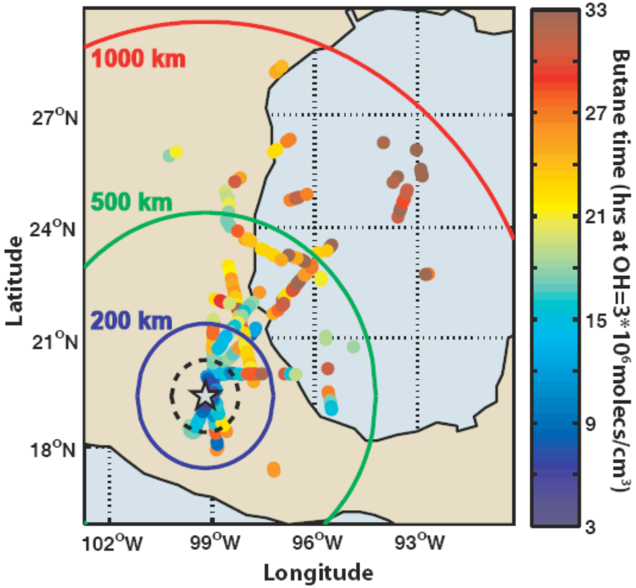

Fig. 2. Locations of data that trace back to the region around Mexico City colored by their photochemical age in hours of processing at OH=3×10^6 molecules/cm^3. The black star represents the location of Mexico City and the dashed black circle shows the limit of the region we have defined as the Mexico City Area (within 100 km of the city center). The colored circles represent distances from the center of Mexico City of 200 km (blue), 500 km (green) and 1000 km (red).

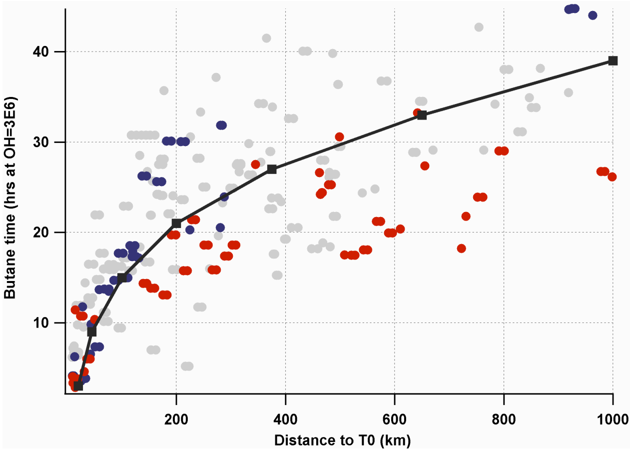

Fig. 3. The relationship between the age calculated from the ratio of 2-butylnitrate to n-butane and the distance to the T0 site in the center of Mexico City. Gray points show all data that traces back to Mexico City, red points represent DC-8 Flight 7 and blue points represent DC-8 Flight 8. The black line shows the average relationship.

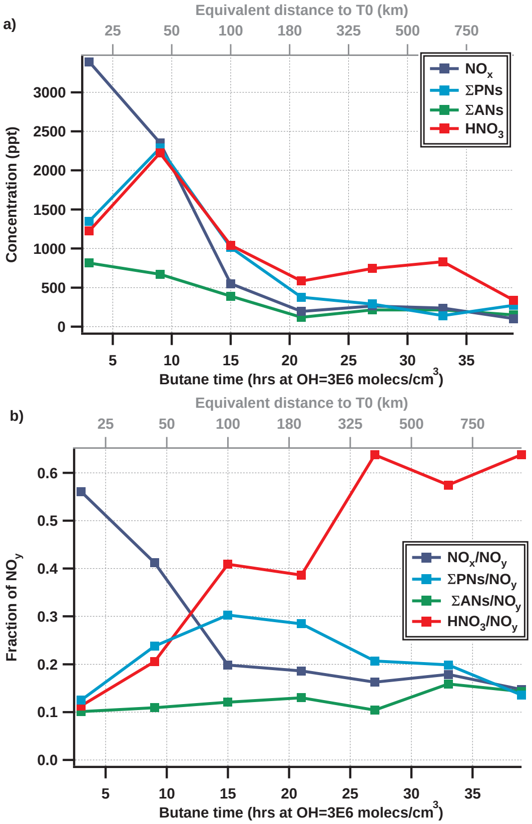

Fig. 4. **(a)** Observed concentrations of the components of NO_y as a function of photochemical age. **(b)** Observed fraction of NO_y comprised of each of the NO_y reservoirs as a function of photochemical age.

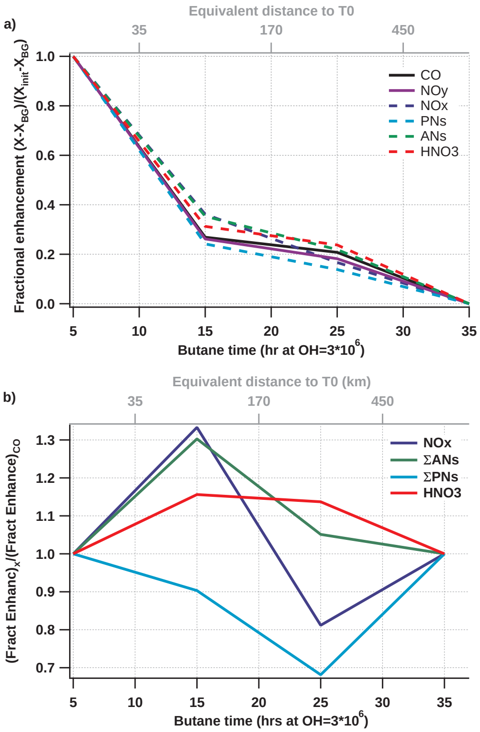

Fig. 5. **(a)** Fractional enhancement of CO (black solid), NO_y (purple solid), NO_x (dotted dark blue), ΣPNs (dotted cyan), ΣANs (dotted green) and HNO_3 (dotted red) used to assess possible impacts of deposition. Background levels are assumed to be equal to levels observed at the most aged point. The overall change is the change from the least aged to most aged points. See text for more description. **(b)** Dilution of the various NO_y reservoirs relative to CO defined as (Fractional enhancement of X)/(Fractional enhancement of CO). NO_x is shown in dark blue, ΣPNs in light blue, ΣANs in green and HNO_3 in red.

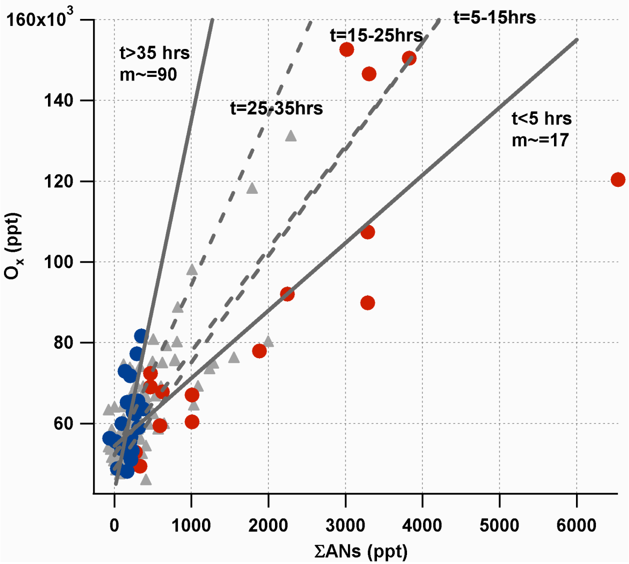

Fig. 6. Observed slopes of ΣANs vs. O_x throughout the plume. The freshest points (photochemical age<5 h) are shown in red and the most aged points (photochemical age>35 h) are shown in blue. The solid lines represent the best fit lines observed for these two sets of data and the dotted lines represent the best fit lines observed at intermediate photochemical ages.

Title Page
Abstract
Introduction
Conclusions
References
Tables
Figures
◀◀
▶▶
◀
▶
Back
Close
Full Screen / Esc
Printer-friendly Version
Interactive Discussion

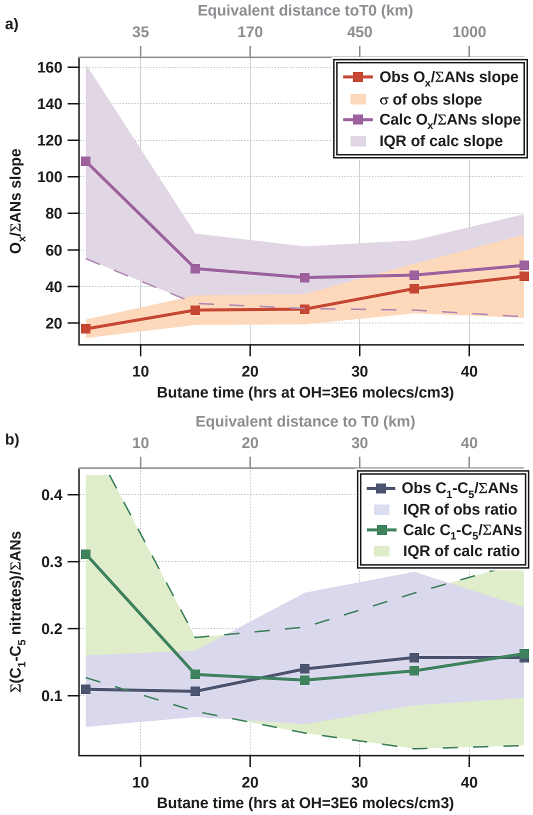

Fig. 7. **(a)** The observed (red) and calculated (purple) ΣANs vs. O_x slope as a function of photochemical age. **(b)** The observed (blue) and calculated (green) $\Sigma(C_1-C_5$ nitrates)/ΣANs ratio as a function of photochemical age.

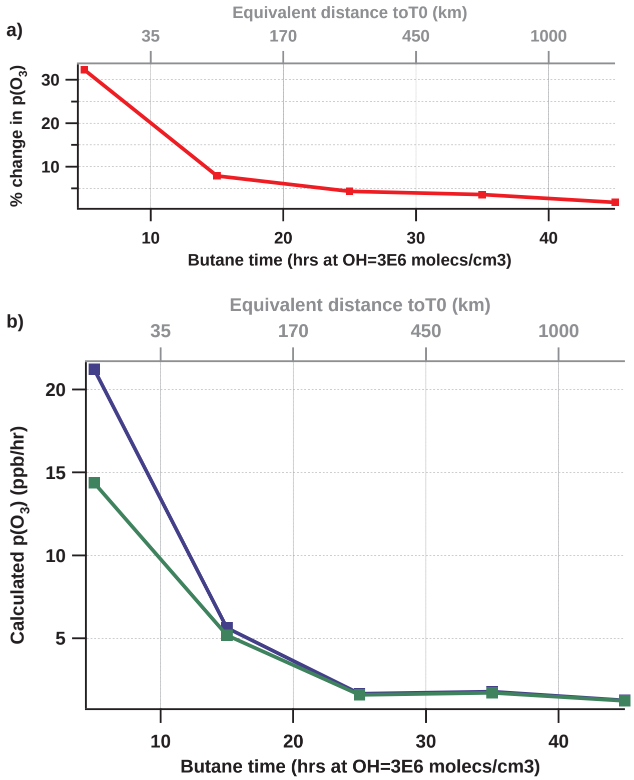

Fig. 8. (a) The percent decrease in the calculated P(O_3) as a result of including ΣANs formation with the observed average nitrate branching ratios. **(b)** The absolute ozone production rate calculated using Eqs. (7 and 8) with (green) and without (blue) consideration of ΣANs formation.